

## Toward Better Constrained Scattering Models for Natural Ice Crystals in the Visible Region

Guanglang Xu<sup>1</sup> , Fritz Waitz<sup>1</sup>, Shawn Wagner<sup>1</sup>, Franziska Nehlert<sup>1</sup>, Martin Schnaiter<sup>1</sup> , and Emma Järvinen<sup>1</sup> 

<sup>1</sup>Karlsruhe Institute of Technology, Karlsruhe, Germany

### Key Points:

- A method is developed for analyzing in-situ polar nephelometer measurements, aiming for constraining the light scattering models for natural ice crystal
- Validity of the method is demonstrated by geometric-optics ray-tracing simulations and in-situ measurements
- A case study of rimed crystals measured in-situ during two aircraft field campaigns using the Particle Habit Imaging and Polar Scattering probe is presented

### Correspondence to:

G. Xu and E. Järvinen,  
[guanglang.xu@kit.edu](mailto:guanglang.xu@kit.edu);  
[emma.jarvinen@kit.edu](mailto:emma.jarvinen@kit.edu)

### Citation:

Xu, G., Waitz, F., Wagner, S., Nehlert, F., Schnaiter, M., & Järvinen, E. (2023). Toward better constrained scattering models for natural ice crystals in the visible region. *Journal of Geophysical Research: Atmospheres*, 128, e2022JD037604. <https://doi.org/10.1029/2022JD037604>

Received 4 AUG 2022  
 Accepted 22 DEC 2022

### Author Contributions:

**Conceptualization:** Guanglang Xu  
**Data curation:** Fritz Waitz, Shawn Wagner, Franziska Nehlert, Martin Schnaiter, Emma Järvinen  
**Formal analysis:** Guanglang Xu  
**Funding acquisition:** Martin Schnaiter, Emma Järvinen  
**Investigation:** Guanglang Xu  
**Methodology:** Guanglang Xu  
**Project Administration:** Martin Schnaiter, Emma Järvinen  
**Resources:** Guanglang Xu, Martin Schnaiter, Emma Järvinen  
**Software:** Guanglang Xu, Fritz Waitz, Emma Järvinen  
**Validation:** Guanglang Xu, Fritz Waitz

© 2023. The Authors.

This is an open access article under the terms of the [Creative Commons Attribution License](https://creativecommons.org/licenses/by/4.0/), which permits use, distribution and reproduction in any medium, provided the original work is properly cited.

**Abstract** In this work, we introduce a method for constraining the optical scattering models of natural ice crystals based on in-situ measurements. Specifically the measured angular scattering functions for ice crystals can be used to compute a set of the asymmetry parameter ( $g$ ) and the corresponding complexity parameter ( $C_p$ ). It is demonstrated that the  $g$ - $C_p$  relation can give valuable information on the morphology of ice crystal. The validity of the methods is shown from theoretical perspectives and the geometric-optics ray-tracing simulations. As an application, we investigate rimed ice crystals from in-situ measurements and found that (a) the  $C_p$  parameter is very well correlated with the surface riming degree and (b) only those models with both roughness and internal scattering can explain the observed  $g$ - $C_p$  relation for rimed particles.

**Plain Language Summary** Light scattering models of ice crystals are important for remote sensing and climate studies. Yet, many physical parameters, such as shape, aspect ratio, and inhomogeneity of the ice crystal can impose significant uncertainty in the single-scattering properties predicted by light scattering models. To reduce such uncertainty and constrain the physical parameters in modeling, we introduce a novel method by analyzing the in-situ measurement of the phase functions of ice crystals. We demonstrate the validity and usefulness of the method using both geometric ray-tracing simulations and a case study on rimed crystals from two campaigns.

## 1. Introduction

When viewing from space, perhaps the most prominent feature of the Earth and the atmosphere is clouds. Clouds play a dominant role in weather, climate and energy balance of the Earth-atmosphere system. Cirrus clouds are composed of ice crystals occupying mostly the upper troposphere. At any given moment, cirrus clouds can cover around 40%–60% of the Earth's surface (e.g., Sassen et al., 2008; Mace et al., 2009; Matus & L'Ecuyer, 2017). Because of their high altitude, cirrus clouds contribute significantly to the reflection of solar radiation, and therefore their radiative properties are crucial in determining the energy budget of the Earth (Baran, 2012; Liou, 1986, 1992; Liou & Yang, 2016; Stephens et al., 1990). A fundamental question for better understanding the radiative properties of cirrus clouds is to accurately model the single-scattering and absorption properties of ice crystals in the solar and infrared spectral regions. Accurate modeling of the optical scattering properties of ice crystals not only improves the representation of cirrus clouds in climate or weather forecasting models, but also helps obtain better retrieval of cloud properties by means of remote sensing (Baran & Labonnote, 2007; Baran et al., 2014; Labonnote et al., 2000; Yang et al., 2018). On a global scale, remote sensing is necessary for gaining important knowledge of cloud properties.

Unlike water droplets in clouds, ice crystals are usually non-spherical and could have complex morphologies. For water droplets, an analytical theory, the Lorenz-Mie theory, can be applied to obtain the single-scattering properties conveniently. Efficient Mie algorithms are available for simulating the light scattering of spherical particles (Wiscombe, 1980). For non-spherical particles, however, there is no such universal tool so far. To better model the scattering properties of non-spherical particles, great effort has been invested toward the development of advanced computational methods. These methods generally are composed of two categories: (a) the numerical accurate methods, such as the Invariant Embedding T-Matrix (II-TM) methods, the Discrete-Dipole Approximation method (DDA), Finite-Difference Time Domain (FDTD) method, and the boundary-element method (Bi & Yang, 2014; Groth et al., 2015; Kleanthous et al., 2022; Mano, 2000; Mishchenko et al., 1996; Taflove & Umashankar, 1990; Yang & Liou, 1996a; Yurkin et al., 2007) and (b) the geometric-optics methods, such as the Convolutional Geometric-Optics Method (CGOM), the Improved Geometric Optics Method (IGOM), and

**Visualization:** Guanglang Xu, Franziska Nehlert, Emma Järvinen

**Writing – original draft:** Guanglang Xu

**Writing – review & editing:** Guanglang Xu, Shawn Wagner, Emma Järvinen

physical optics methods (Borovoi & Grishin, 2003; Hesse, 2008; Macke, Mueller, & Raschke, 1996; Yang & Liou, 1996b).

Thanks to the improved numerical modeling capabilities, our understanding of the light scattering properties of ice crystals with complex particle morphology has been improved dramatically. By applying the geometric-optics method, Macke, Mueller, and Raschke (1996) investigated the optical scattering properties of hexagonal ice crystals with distorted facets. Yang and Liou (1998) investigated the scattering properties of complex ice crystals by employing a surface roughness model. Additionally, the light scattering properties of ice crystals with inclusions have been studied (Macke, Mishchenko, & Cairns, 1996; Panetta et al., 2016; Tang et al., 2017). Apart from the canonical hexagonal models, many other complex shape models have been proposed, such as the Koch fractals (Macke, Mueller, & Raschke, 1996), Voronoi particle (Letu et al., 2016), Gaussian roughness on random spheres (Nousiainen & McFarquhar, 2004; Nousiainen & Muinonen, 2007; Um & McFarquhar, 2011) and particles prescribed by Chebyshev polynomial series (McFarquhar et al., 2002).

It should be noted that the difficulty of light scattering by non-spherical particles not only lies in the technical aspects of developing advanced computational methods, but also lies in the fact that there are many physical parameters that can have impacts on their light scattering properties. According to previous modeling studies, the light scattering properties of ice crystals could depend on *particle shape*, *aspect ratio*, *surface roughness*, *air/aerosol inclusion*, and *orientation* etc. To put it in a more abstract way, the “*parameter space*” is much larger than in the case of spherical particles. Nevertheless, these parameters must be properly constrained in order to obtain accurate representation of the real natural ice clouds. One well-known example is that the 22° and 46° halos predicted by smoothed hexagonal models are rarely seen in real clouds. In addition, according to geometric-optics ray-tracing simulations, the asymmetry parameter of a large hexagonal column or plate can vary from 0.65 to about 0.9 by just changing the aspect ratio and surface roughness of the model (Um et al., 2015; Xu et al., 2022). By including the internal scatter, the asymmetry parameter can be further reduced to around 0.5 (Macke, Mishchenko, & Cairns, 1996; Tang et al., 2017). It is conceivable that, without proper constraints on the light scattering models, large errors could be introduced in either climate or remote sensing applications involving ice clouds.

Understanding the relation between particle morphology and their optical scattering properties is a fundamental question in electromagnetic scattering by non-spherical particles. Much of the work on this topic is done by theoretical and modeling approaches. The book by Mishchenko et al. (2002) provides in-depth discussion and synthesis of works on the topic. Nonetheless, the constraint of the physical parameters involving natural ice crystals can only be obtained by a joint effort of measurement and modeling. For instance, by applying both a ray-tracing model and the in-situ polar nephelometer measurements, Shcherbakov et al. (2005) found that the surface roughness model with Weibull statistics (Dodson, 1994) in general give more reasonable explanation on the measured angular scattering intensity than the original model proposed by Macke, Mueller, and Raschke (1996). By the analysis of in-situ measured angular scattering intensities of ice crystal ensembles using Legendre polynomials, Xu et al. (2022) found that the real ice crystals in an Arctic cirrus case study had a much higher complexity than the idealized models. Additionally, Tang et al. (2017) found that by using models that have both surface roughness and air inclusions, the simulated polarized reflectance is most consistent with remote sensing observations. In recent years, remote sensing approaches have been applied to retrieve the physical properties of ice crystals quantitatively, such as surface roughness, distortion parameter, and overall morphology (Hioki et al., 2016; Saito et al., 2017; van Diedenhoven, 2018, 2021). The validity of remote sensing retrieval is nevertheless dependent on the underlying assumptions about cloud geometry and the prior light scattering models.

The overarching goal of this study is to better constrain the optical scattering models for climate or remote sensing studies by means of in-situ polar nephelometer measurements. In contrast to remote-sensing approaches, in-situ measurements are the most direct method for measuring angular light scattering properties of atmospheric ice crystals, by which many of the assumptions can be avoided. Specifically, we propose the so-called  $C_p$ -analysis for a better understanding of the relation between the scattering phase function and the particle morphological complexity. We first present some theoretical explanations on the concept of the  $C_p$  parameter and demonstrate its effectiveness in analyzing the scattering phase function using geometric-optics ray-tracing models. In the case study, we analyze the in-situ data associated with rimed ice crystals. The data are collected from the Particle Habit Imaging and Polar Scattering (PHIPS) probe (Abdelmonem et al., 2016; Schnaiter et al., 2018). A significant advantage of the PHIPS instrument is that it simultaneously measures microscopic stereo-images and the angular

scattering intensity in the polar angular range of  $18^\circ$ – $170^\circ$  for single particles. In such a way, the linkage between the particle morphology and optical scattering properties can be analyzed. Together with geometric-optics modeling, we demonstrate the usefulness of the approach in constraining the light scattering models.

The structure of the paper is as follows: in Section two we introduce the conceptual and theoretical basics for this study. Section three introduces the so-called  $C_p$ -analysis for complex light scattering models. To validate the theoretical and modeling analysis, in Section four, we discuss a case study on rimed ice crystals from in-situ measurements. Section five concludes this study.

## 2. Theoretical Basics

The scattering phase function for a particle generally contains rich information about its morphology. For instance, the rainbow feature in the scattering phase function is caused by the sphericity of the particle. The  $22^\circ$  and  $46^\circ$  halo feature can be explained by the light ray refracted through the prism angles of  $60^\circ$  and  $90^\circ$  formed by the facets in the hexagonal column or plate. It is therefore meaningful to develop methods for retrieving the morphology from the observed scattering phase function. Such a problem can be considered as an inverse-scattering problem. In the development of an algorithm for retrieving the asymmetry parameter from the measurements of a polar nephelometer, Xu et al. (2022) introduced a so-called  $C_p$  parameter that describes the smoothness and isotropic degree of the phase function. It is defined as:

$$C_p = \left( \sum_{l=0}^{\infty} |\hat{c}_{GO,l}| \right)^{-1}, \quad (1)$$

where  $\hat{c}_{GO,l}$  is the expansion coefficients of phase function due to the *reflection–refraction* of light ray (without forward diffraction) by using a series of Legendre polynomials  $P_l(\cos(\Theta))$ , that is,

$$P_{GO}(\Theta) = \sum_{l=0}^{\infty} (2l+1) \hat{c}_{GO,l} P_l(\cos(\Theta)). \quad (2)$$

It was found that the  $C_p$  parameter is closely connected to the distortion parameter  $\delta$  proposed by Macke, Mueller, and Raschke (1996). The algorithm for retrieving  $C_p$  from polar nephelometer measurement is described in Xu et al. (2022). Note that the first coefficient  $\hat{c}_{GO,0}$  is set to be:

$$\hat{c}_{GO,0} = 1, \quad (3)$$

such that the integral of the intensity is normalized properly. In addition,  $C_p$  must fall in the range between 0 and 1, that is,

$$0 \leq C_p \leq 1, \quad (4)$$

where the case of 0 corresponds to a Dirac-delta function (i.e., no scattering) and 1 corresponds to isotropic scattering. For a delta function, its Legendre expansion is as follows,

$$2\delta(1 - \cos(\theta)) = \sum_{l=0}^{\infty} (2l+1) P_l(\cos(\theta)), \quad (5)$$

meaning  $\hat{c}_{GO,l} = 1$  for all  $l$ , which makes the value of  $C_p$  infinitely close to *zero*. On the other hand, for a constant phase function, we have:

$$\hat{c}_{GO,l} = \begin{cases} 1 & \text{if } l = 0, \\ 0 & \text{if } l > 0, \end{cases}$$

which leads to  $C_p = 1$ . In some sense, the  $C_p$  parameter measures the “distance” between arbitrary scattering phase function and a Dirac-delta function and this “distance” varies from 0 to 1.

A common practice in characterizing the anisotropic degree of a scattering phase function  $P(\Theta)$  is to use asymmetry parameter,

$$g = \int_0^\pi P(\Theta)\cos(\Theta)\sin(\Theta)d\Theta. \quad (6)$$

For instance, an isotropic phase function has an asymmetry parameter value of *zero*, and when  $g$  is very close to *one*, it is evident that the phase function will be highly-forward peaked. Such characteristics can be seen from a commonly applied analytical phase function called Henyey-Greenstein (HG) phase function (Henyey & Greenstein, 1941; van de Hulst, 1980), which were originally used to describe the light scattering by interstellar dust clouds:

$$P_{HG} = \frac{1 - g^2}{(1 + g^2 - 2g\cos(\Theta))^{3/2}}, \quad (7)$$

which has a simple form of expansion coefficient with respect to Legendre polynomials:

$$\hat{c}_{HG,l} = g^l. \quad (8)$$

When  $g = 0$  the HG phase function will reduce to a constant phase function, and when  $g$  is close to *one*, the phase function is close to a delta function. Applying the definition of  $C_p$  to HG phase function and use the following geometric series formula,

$$\frac{1}{1 - |g|} = \sum_{l=0}^{\infty} |g|^l, \quad (9)$$

we have a very simple relation between  $g$  and  $C_p$ , that is,

$$C_p + |g| = 1. \quad (10)$$

Additionally, for two phase functions  $P_1(\Theta)$  and  $P_2(\Theta)$  satisfying

$$P_1(\Theta) = P_2(\pi - \Theta), \quad (11)$$

their  $C_p$  values must be equal. This can be shown readily. Let the expansion coefficient for  $P_1(\Theta)$  and  $P_2(\Theta)$  be  $\chi_{1,l}$  and  $\chi_{2,l}$  respectively, by using a basic property of Legendre polynomials, that is,

$$P_l(-\cos(\Theta)) = (-1)^l P_l(\cos(\Theta)), \quad (12)$$

we have

$$\chi_{1,l} = (-1)^l \chi_{2,l}, \quad (13)$$

meaning that their  $C_p$  values must be the same. Due to these properties, in contrast to  $g$ , the  $C_p$  parameter can be considered as a “symmetry parameter” of the phase function. Figure 1 shows the HG phase functions with different asymmetry parameters and corresponding  $C_p$  parameters.

To better understand the physical meaning of  $C_p$  parameter, we discuss some other aspects of  $C_p$  and its relevance in light scattering under the framework of Monte-Carlo ray-tracing. If a Monte-Carlo ray-tracing technique is employed, the light ray will undergo many scattering events before it gets detected by a detector. Therefore any ray-tracing process can be loosely interpreted from the point of view of multiple scattering. Particularly, under the framework of successive order of scattering (SOS) (Lenoble, 1985), the diffuse radiance can be expressed as

$$I(\Omega) = \sum_{s=0}^{\infty} I_s(\Omega), \quad (14)$$

where  $s$  denotes the order of scattering, and  $\Omega$  is the scattering direction with respect to a spherical coordinate. In such a way, the incident beam angular distribution profile (a Dirac-delta function) can be seen as a *zero-order* “scattering” phase function. The first external-reflection event could be considered as the “first-order” scattering event and so on. As the inclusion of any internal scatter increases, for instance, higher-order scattering becomes more important. Examining the formula of SOS, one can find that the angular distribution of the radiance associated with  $s$ -order scattering is related to  $s$ -fold convoluted phase function, that is,

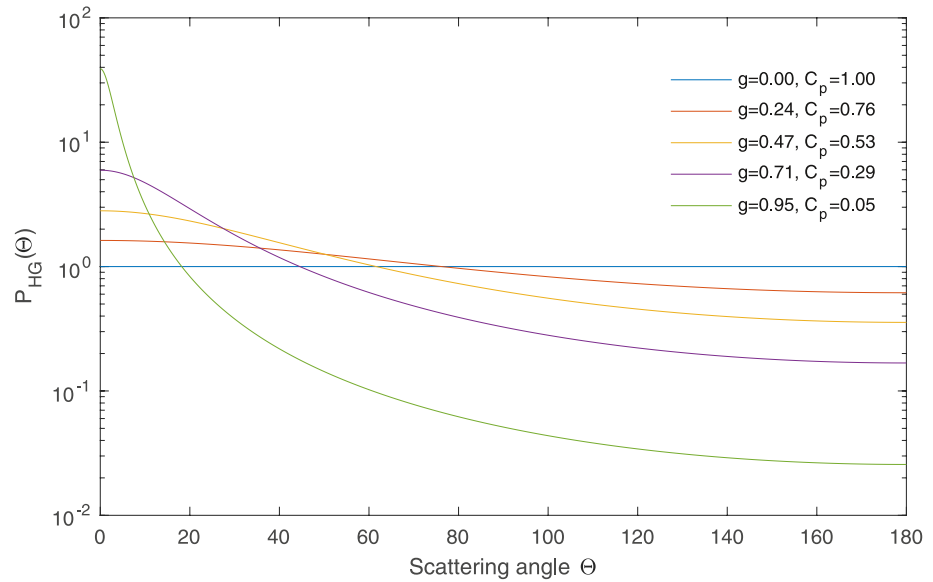


**Figure 1.** The  $C_p$  parameter and the corresponding asymmetry parameter for the Henyey-Greenstein phase functions.

$$I_s(\mathbf{\Omega}) \sim P_s(\mathbf{\Omega}_0, \mathbf{\Omega}), \quad (15)$$

where  $\mathbf{\Omega}_0$  is the incident direction and  $P_s(\mathbf{\Omega}_0, \mathbf{\Omega})$  is the  $s$ -fold convoluted phase function,

$$P_s(\mathbf{\Omega}_0, \mathbf{\Omega}) = \int_{\mathbf{\Omega}'} P_{s-1}(\mathbf{\Omega}_0, \mathbf{\Omega}') P(\mathbf{\Omega}, \mathbf{\Omega}') d\mathbf{\Omega}', \quad (16)$$

Let us use the specified the direction  $\mathbf{\Omega}$  with coordinates  $(\mu, \phi)$ , where  $\mu$  is the cosine of the zenith angle and  $\phi$  is azimuthal angle. Equation 16 can be written as (Efremenko & Kokhanovsky, 2021)

$$P_s(\mu_0, \mu, \phi) = \sum_{m=0}^{\infty} (2 - \delta_{m0}) \sum_{n=m}^{\infty} \chi_n^s \bar{P}_n^m(\mu_0) \bar{P}_n^m(\mu) \cos(m\phi), \quad (17)$$

where  $\bar{P}_n^m(\mu)$  is the associated Legendre function and  $\chi_n$  is the expansion coefficients of scattering phase function  $P(\Theta)$  with respect to Legendre polynomials. It is sufficient to consider the azimuthal averaged case, that is,  $m = 0$ , and set  $\mu_0 = 1$ , then the above equation can be written as:

$$\bar{P}_s(\mu_0, \mu) = \sum_{n=0}^{\infty} (2n + 1) \chi_n^s P_n(\mu). \quad (18)$$

It can be seen that for  $s$ -order scattering phase function, the expansion coefficients  $\chi_n$  simply become  $\chi_n^s$ . The  $C_p$  parameter for order- $s$  scattering phase function  $C_p(s)$  is

$$C_p(s) = \left( \sum_{l=0}^{\infty} |\chi_l^s| \right)^{-1}. \quad (19)$$

This means the decay rate of the coefficients become faster and therefore leads to a more isotropic phase function. In other words, as the order of scattering increases, the scattered radiance will become more isotropic. According to the definition of  $C_p$  and Equation 15, the enhancement of higher-order scattering will increase the value of  $C_p$ . If the multiple-scattering effects are small, it is conceivable that the angular feature of the radiance distribution and the  $C_p$  value will be determined by the first few orders of scattering and the corresponding scattering phase functions. If high-order scattering contribution is strong, then the scattering radiance will tend to be more isotropic and less dependent on the phase function itself.

Figure 2 displays the behavior of  $C_p$  and a scattering phase function according to the perspective of SOS based on Equation 18. The “1st-order” phase function is computed from a ray-tracing method using a hexagonal column.

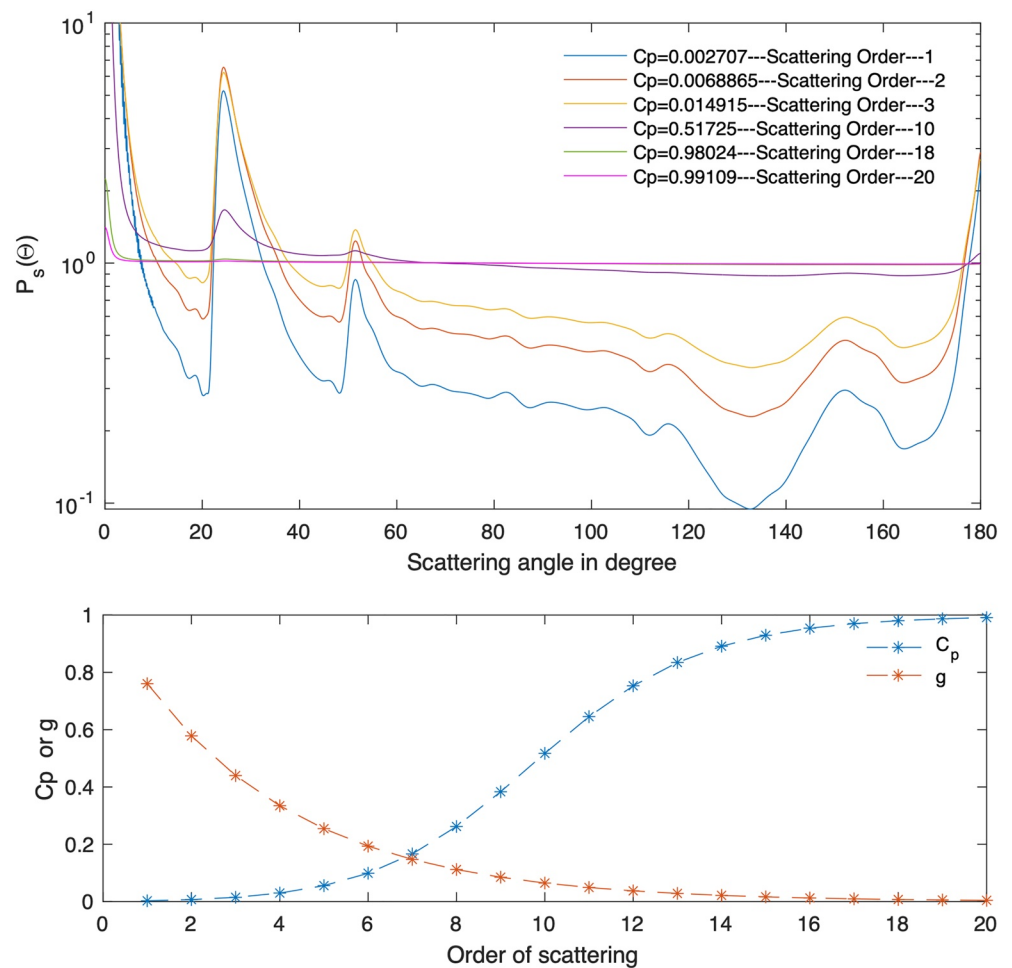


**Figure 2.** Interpretation of  $C_p$  parameter from the perspective of successive order of scattering.

The length of the hexagonal column is  $100 \mu\text{m}$  and the radius of the base facet is  $50 \mu\text{m}$  at the wavelength of  $0.532 \mu\text{m}$ . The refractive index used for the simulation is  $1.33 + 0i$ . As the order of scattering increases, the angular features (i.e.,  $22^\circ$  and  $46^\circ$  halos) of the phase function is suppressed, as shown in the upper panel of Figure 2. The lower panel of the figure shows the increase of  $C_p$  and decrease of  $g$  as the order of scattering increases. Because  $C_p$  is determined by all the expansion coefficients of a phase function, it can be used to measure the “similarity” of phase functions. It is clear that the phase function will be “similar,” or less sensitive to the increase of order of scattering when the number of scattering order is very small (e.g., 1st to 3rd) or very large (e.g., 18th to 20th). This can also be seen in the upper panel, showing the phase functions for different orders of scattering. Clearly, the  $C_p$  parameter with respect to the total radiance (14) can be used to measure the degree of multiple-scattering. Specifically, a small  $C_p$  corresponds to a weak multiple scattering effect and a large  $C_p$  suggests a strong multiple scattering effect. Surprisingly, the increasing rates of  $C_p$  are quite similar for both the very-low-order-scattering-dominated region (e.g., 1st to 3rd) and the very-high-order-scattering-dominated region (e.g., 18th to 20th). The asymmetry parameter shows an exponential decay curve as revealed by Equation 18. In the region of small  $C_p$  (i.e., weak multiple scattering), the asymmetry parameter is more sensitive to the increase of scattering order, whereas in the region of large  $C_p$  (i.e., strong multiple scattering region), the asymmetry parameter decreases slowly. It should be noted that the above discussion only concerns about how  $C_p$  and  $g$  could possibly change due to different orders of scattering according to Equation 14, one might also use other phase functions (such as phase function for an air bubble) to visualize this effect, but it does not correspond to any particular solution of light scattering problems when  $s > 1$ .

Based on above analysis, it can be seen that the  $C_p$  parameter is well-defined and has a clear physical meaning under the framework of SOS. Its variation pattern, in connection with other parameters (e.g., asymmetry

parameter) could provide us useful information regarding the light-scattering properties of a particle and is worth studying from both theoretical and experimental points of view.

### 3. The $C_p$ -Analysis for Complex Ice Crystal Models

Before we proceed to any real data, in this section we discuss various optical scattering models with different complexity metrics and their relations to the  $C_p$  parameter. It should be noted that this study is restricted to the geometrical-optics region, where the size parameter is generally  $>50$  (Xu et al., 2022). And because we are focusing on conventional ray-tracing methods, the wave-interference effects (could potentially enhance back-scattering, see e.g., Zhou, 2018) are not considered in the computation of  $C_p$  parameter. Nevertheless, the concept of  $C_p$  is obviously independent of any numerical methods. Since the  $C_p$  is measurable by a polar nephelometer, the analysis can be applied to in-situ or laboratory measurements. Additionally, the computational methods applied in the study have been widely applied in previous studies, and the accuracy have been verified by comparing with numerical accurate methods (Macke et al., 1995; Yang et al., 2019).

#### 3.1. The Morphological Complexity Metrics of Ice Crystals

Although a typical hexagonal shape model is widely applied for light scattering modeling, such idealized pristine hexagonal shapes are rarely seen from in-situ measurements (Lawson et al., 2019). On the contrary, the majority of atmospheric ice crystals are classified as having “irregular” shapes or having sub-micron scale morphological complexity (Järvinen, Jourdan, et al., 2018, Järvinen, Wernli, & Schnaiter, 2018; Ulanowski et al., 2014). It is therefore meaningful to devise some quantitatively well-defined metrics to better characterize ice crystal morphological complexity and the respective optical scattering effects. Such metrics can also be termed as the “optical complexity metric.”

The light scattering by large irregular particles can be treated most effectively by applying geometric-optics ray-tracing methods. For modeling the light scattering properties of imperfect hexagonal ice crystals, Macke, Mueller, and Raschke (1996) introduce a statistical local distortion of the crystal facets. Specifically, the local normal of a crystal facet is tilted randomly from its original direction in the scattering process. The zenith and azimuth tilt angles are chosen randomly from the intervals  $[0, \theta_{\max}]$  and  $[0, 2\pi]$ . As such, the optical complexity, or the distortion parameter  $\delta$  can be defined as:

$$\delta = \theta_{\max}/90^\circ. \quad (20)$$

Note that the  $\theta_{\max}$  can only reach to a maximum value of  $90^\circ$ , therefore the distortion parameter must satisfy the following,

$$0 \leq \delta \leq 1. \quad (21)$$

Similarly, Yang and Liou (1998) employed a geometric-optics method with a basic assumption that the real ice crystals are rough and consist of a large number of microscopic facets. These facets are locally planar and randomly tilted from the orientations in the case of a smooth surface. The distribution of the slopes was assumed to be isotropic and Gaussian with a mean-square of  $\sigma^2/2$ . More specifically, the facets are tilted randomly according to the distribution

$$P(Z_x, Z_y) = \frac{1}{\sigma^2 \pi} \exp\left(-\frac{Z_x^2 + Z_y^2}{\sigma^2}\right), \quad (22)$$

where (as described above)  $Z_x$  and  $Z_y$  are local gradients of the surface height in the  $x$  and  $y$  directions and  $\sigma$  is a complexity parameter controlling the degree of roughness. Based on simulations, it is evident that the surface roughness controlled by the above parameters can exert strong effects on diminishing the features of the scattering phase functions, especially on the  $22^\circ$  and  $46^\circ$  halos. Detailed discussion on the impacts of surface roughness on the scattering phase matrix elements can be seen in Yang and Liou (1998), Macke, Mueller, and Raschke (1996) and Hess et al. (1998).

Another different type of complexity of ice crystals is the internal scattering due to, for example, air inclusions. The simulation of such effects for large particles can only be realized practically through Monte-Carlo ray-tracing

methods. An important concept in this approach is the so-called mean free path. Specifically, the light ray, after being refracted into the particle, is allowed to travel a free path length  $l$  without encountering any internal scatter:

$$l = -\bar{l} \times \log(R(0, 1)), \quad (23)$$

where  $\bar{l}$  is the mean free path of the light ray and  $R(0, 1)$  denotes an equally-distributed random number between 0 and 1. If the photon does not reach the boundary of the particle, its propagation will be redirected according to the scattering phase function of the internal scatter. The absorption of the scatter can also be taken into account by specifying a single scattering albedo  $\bar{\omega}_{incl}$ . More technical details can be seen from Macke, Mishchenko, and Cairns (1996) and Tang et al. (2017). It should be noted that it is not the purpose of this study to examine all the complexity metrics for modeling the light scattering properties of ice crystals. Instead, we focus on the commonly used complexity metrics that can be applied to a basic hexagonal geometry in the geometric-optics regime.

### 3.2. The Relation Between $C_p$ and Complexity Metrics

The parameters introduced above have been employed to the study of the radiative impact of ice clouds. Ice crystal complexity plays an important role in the radiative budget of the Earth-atmosphere system (Järvinen, Jourdan, et al., 2018; Yi, 2022; Yi et al., 2013). A common practice of such investigation is to change the radiation parameterization scheme in a climate model in accordance with the complex models of ice crystals so climate impact can be subsequently evaluated. Nevertheless, the knowledge on degree of complexity of real atmospheric ice crystals still remains an area of active research. One way to address the problem is from in-situ or laboratory measurements.

The utilization of the  $C_p$  parameter for characterizing scattering phase function has many advantages. First of all, the  $C_p$  parameter is mathematically well defined. The  $C_p$  parameter takes in all the expansion coefficients associated with Legendre polynomials, therefore it contains richer information than asymmetry parameter. Due to this property, it can measure not only the overall isotropic degree of the phase function (asymmetry parameter is also useful in this respect), but also measure the local smoothness of the phase function (asymmetry parameter cannot measure the local features). Second and more importantly, the  $C_p$  parameter can be retrieved from in-situ or laboratory light scattering measurement. Due to its measurability, the  $C_p$  value can serve as the link between modeling and measurement for complex non-spherical particles. These significant advantages make it meaningful to explore the relation between  $C_p$  and different complexity metrics for light scattering models.

A common practice in studying light scattering models for ice crystals is to compare the scattering phase function. Due to the fact that the forward scattering intensities are often much larger than that of the side-scattering angles, phase functions are often plotted in logarithmic scale. The upper right panel of Figure 3 shows the geometric-optics ray-tracing part of the phase function (i.e., the reflection-refraction of light rays) for different hexagonal models with various degrees of surface roughness  $\sigma$  from 0.1 to 1.0. The model sizes and aspect ratios are shown in the legend of the lower right panel. With all these curves in logarithmic scale, perhaps the only information we can readily obtain from the upper part of Figure 3 is that increasing the surface roughness can diminish the 22° and 46° halo features.

The lower right panel shows the corresponding  $C_p$  values for the geometrical-optics phase functions for different models as a function of surface roughness. Clearly, increase of surface roughness parameter  $\sigma$  will increase the magnitude of  $C_p$ , making the phase function smoother and featureless. However, it becomes apparent that the increase of  $C_p$  will also become less sensitive to surface roughness parameter  $\sigma$ . This can be seen as some sort of “saturation” of surface roughness model or the convergence of  $C_p$ . Looking back to the upper panel, this “saturation” means the phase function will not be very different as the surface roughness  $\sigma$  varies from 0.9 to 1.0. Unlike the upper right panel, one can easily see this saturation pattern of surface roughness in the lower right panel using  $C_p$ . We also note that the  $\sigma$  roughness model has a maximum  $C_p$  of 0.3, which is slightly lower than observation in a case study of cirrus clouds Xu et al. (2022). In addition, the lower panel also reveals some of the patterns that are hidden in the upper panel, that is, the aspect ratio effects. From the lower panel, we can clearly see that the  $C_p$  value associated with an aspect ratio of one increases faster than other aspect ratios, such as 2 or 0.25. This means that by changing the surface roughness, the phase functions associated with particles with an aspect ratio of one become smoother and more isotropic faster than particles with more extreme aspect ratio. Such information is unlikely to be seen from the conventional phase function comparisons such as shown in the upper panel.

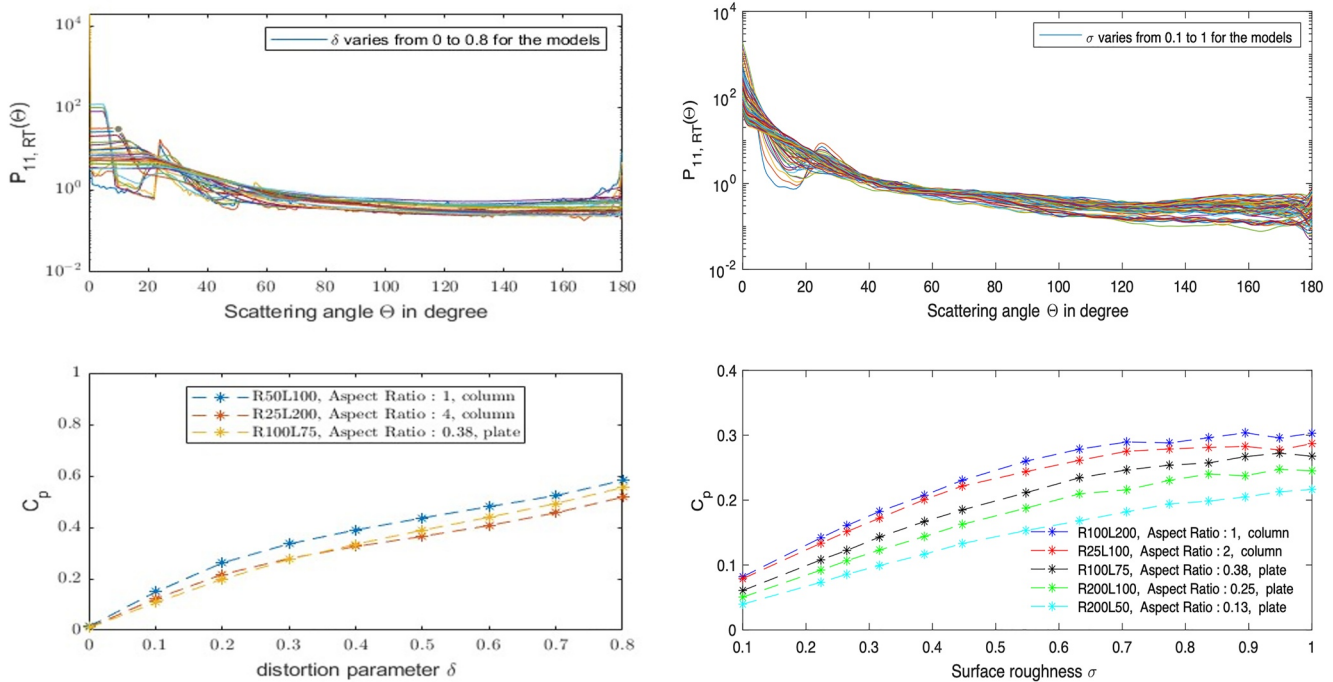


**Figure 3.** Sensitivity of  $C_p$  to surface roughness models from Yang and Liou (1998) and Macke, Mueller, and Raschke (1996).

The left panels of Figure 3 show a similar plot for the hexagonal models based on Macke, Mueller, and Raschke (1996). It can be seen that the correlation between  $C_p$  and the distortion parameter  $\delta$  is very close to a linear relation, and no “saturation” pattern is seen from the relation. This phenomena can be loosely explained by the fact that the outgoing rays in the distortion model Macke, Mueller, and Raschke (1996) are distributed more isotropically than the roughness model  $\sigma$  associated with a Gaussian distribution. As the distortion parameter  $\delta$  increases to 0.8, the  $C_p$  parameter almost linearly increase to between 0.5 and 0.6 for the models. Again, for the distortion model, the particles with an aspect ratio of one will have a  $C_p$  value that increases faster than other aspect ratios, meaning they scatter light-rays more isotropically than extreme-aspect-ratio particles.

The influence of internal scatter on the scattering properties of ice crystals has been investigated using Monte-Carlo ray-tracing methods, for example, in Panetta et al. (2016), Tang et al. (2017) and Macke, Mishchenko, and Cairns (1996). We shall now reanalyze the variations on phase function due to internal scattering through the  $C_p$  parameter. Figure 4 shows simulations of scattering phase function using different mean free path  $l$  parameter for three hexagonal columns with smooth surface. From the upper panel of the figure, it is rather difficult to see how the phase function changes as the amount of internal scatter increases. However, in the lower panel where the  $C_p$  values are plotted, one can clearly see that the inclusion of internal scatters poses strong effects on smoothing the phase function (compared to surface roughness). As the mean free path reduces to about 30  $\mu\text{m}$ , the  $C_p$  for R50L100 model already reaches 0.2, whereas when the mean free path reduces to about 10  $\mu\text{m}$ , the  $C_p$  increases to 0.8. This means that the internal scattering could play a very important role in smoothing the phase function, while surface roughness models such as parameter  $\sigma$  have only minor effects. In addition, we also can find similar “aspect-ratio-effect”, that is, when the aspect ratio is close to one, the  $C_p$  value increases faster. With the help of  $C_p$ -analysis, we can clearly see that this “aspect-ratio-effect” seems to be universal for different complex models. It is conceivable that with the conventional phase-function comparison it is rather difficult to extract these information.

### 3.3. The $g$ - $C_p$ Curves

In order to constrain the light scattering models using measurements, one has to be able to apply the quantities that are measurable. Above we have demonstrated the correlation between the complexity metrics of the particle and the  $C_p$  parameter. Nevertheless, the optical complexity metrics are not measurable directly. Therefore one

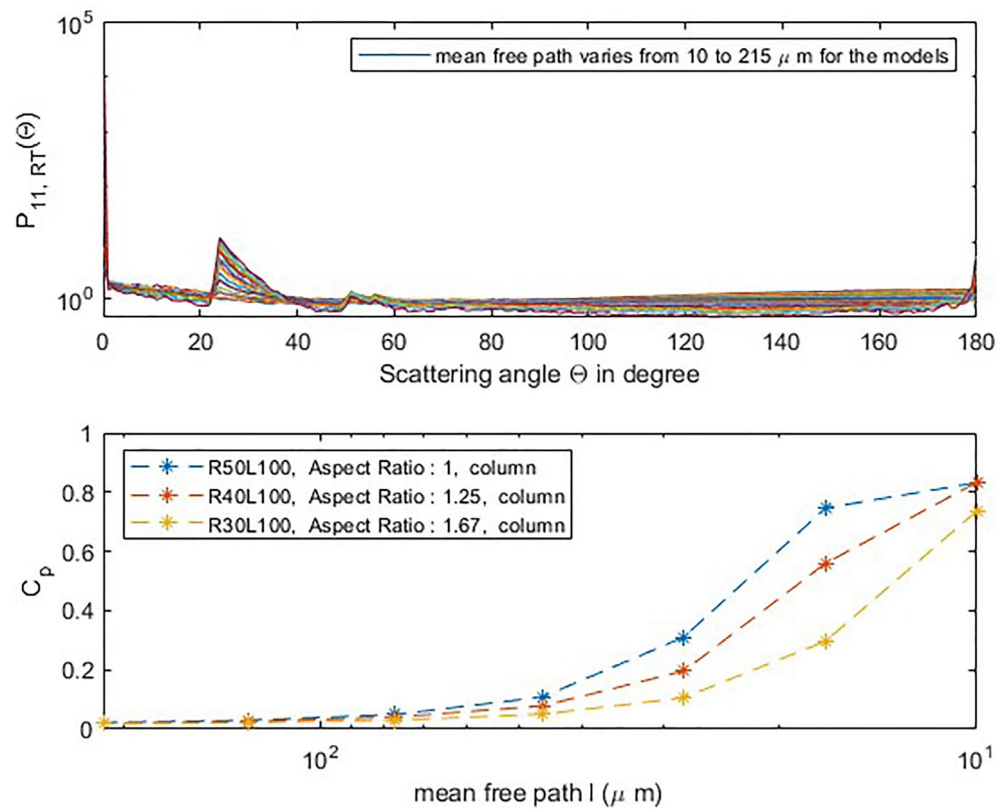


**Figure 4.** Sensitivity of  $C_p$  to mean free path for smooth ( $\delta = 0$ ) hexagonal models from Macke, Mishchenko, and Cairns (1996).

cannot simply apply the above relations and derive useful information. From a statistical perspective, a category of ice particles (e.g., columns or plates) should produce statistically stable scattering signals. It is therefore meaningful to focus on the statistical behavior of the phase-function-changing pattern for a class of model. A useful relation for unlocking this information is how the asymmetry parameter  $g$  varies with the  $C_p$  parameter. It is well-known that the asymmetry parameter will generally decrease as the complexity of the particle increases. From numerical simulations, it has been noticed that, however, when the distortion parameter  $\delta$  is relatively low, the asymmetry parameter is not sensitive to the increase of distortion parameter  $\delta$ . For example, the upper panel of Figure 5 displays the four phase functions with the same asymmetry parameter 0.75 but with different distortion and  $C_p$  parameters. The lower panel shows the absolute value of the expansion coefficients for the corresponding phase functions. The reason that these phase functions share the same asymmetry parameter is that they have the same expansion coefficient for the first degree of Legendre polynomial, and increasing the distortion parameter will only suppress the magnitude of the coefficients of higher order of polynomials, as shown in the lower panel of Figure 5. Nevertheless, for the increase of other complexity, such as air-inclusion, the asymmetry parameter could decrease quite fast. This variation pattern between asymmetry parameter and complexity could be used to distinguish different types of complexity of ice crystals. And since the  $C_p$  parameter can be used to measure the effects of different types of morphological complexity, it is natural to investigate the relation between the asymmetry parameter and the  $C_p$  parameter.

Figure 6 displays how the asymmetry parameter changes with the value of  $C_p$  using distortion parameter  $\delta$ -variation or different mean free-path-length parameters. The upper panel displays how the asymmetry parameter changes as the  $C_p$  parameter increases, and these curves are obtained by adjusting the distortion parameter for a homogeneous ice crystal. The lower panel shows the curves for different models that have only internal scattering without distortion and the mean free path varies from 10 to 215  $\mu\text{m}$ . It can be seen that the  $g$ - $C_p$  curves are very useful in distinguishing the two different models. For homogeneous but roughed models (upper panel), the asymmetry parameter decreases rather slowly (almost constant) in the small  $C_p$  region, and as  $C_p$  gets larger, all

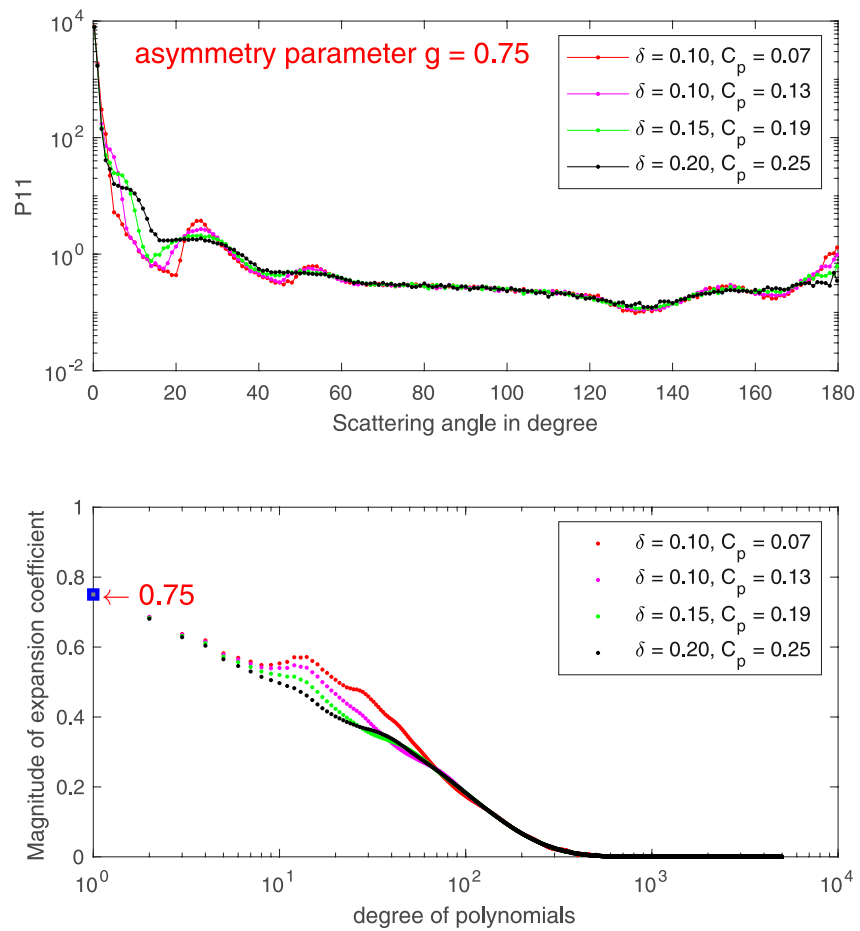


**Figure 5.** (Upper panel) Four phase functions with the same asymmetry parameter 0.75, but with different  $C_p$  and distortion parameters. The model used for the simulation is a hexagonal column with a length of  $100 \mu\text{m}$  and base facet radius of  $50 \mu\text{m}$  at the wavelength of  $532 \text{ nm}$ . (Lower panel) The corresponding magnitude of expansion coefficients for the four phase functions.

the curves converge to a very similar linear decreasing pattern. For smoothed but inhomogeneous particle models (lower panel), the asymmetry parameter decreases rather quickly as  $C_p$  increases from a small value, and as  $C_p$  get larger, the asymmetry parameter decreases rather slowly. Using the theoretical framework of SOS described in section two, the pattern in the upper panel can be explained by lower-order scattering contributions with increasingly isotropic sampling (in the Monte-Carlo ray tracing process). On the other hand, the lower panel can be explained by higher-order scattering contribution as the mean-free-path parameter decreases.

Figure 7 shows the  $g-C_p$  relation for the particles with both roughness and internal scatter simultaneously increase. Surprisingly, these curves are very close to a linear relation. By comparing these curves, one can clearly see that the  $g-C_p$  curves are useful for studying the phase function behaviors of a particular type of model. In other words, the morphological information of the particle, being hidden in the phase function, can be retrieved from the  $g-C_p$  relations. These curves are useful for constraining the optical scattering models for ice crystals, because they are measurable by a polar nephelometer. In the next section, we will present some applications of this method to in-situ measurements.

#### 4. Applications to In-Situ Measurements

To validate our theoretical and modeling analysis, in this section we investigate the correlation between the  $C_p$  parameter and the morphological complexity and the  $g-C_p$  relations for real atmospheric ice crystals derived from polar nephelometer measurements with the PHIPS probe. PHIPS has been developed to measure simultaneously

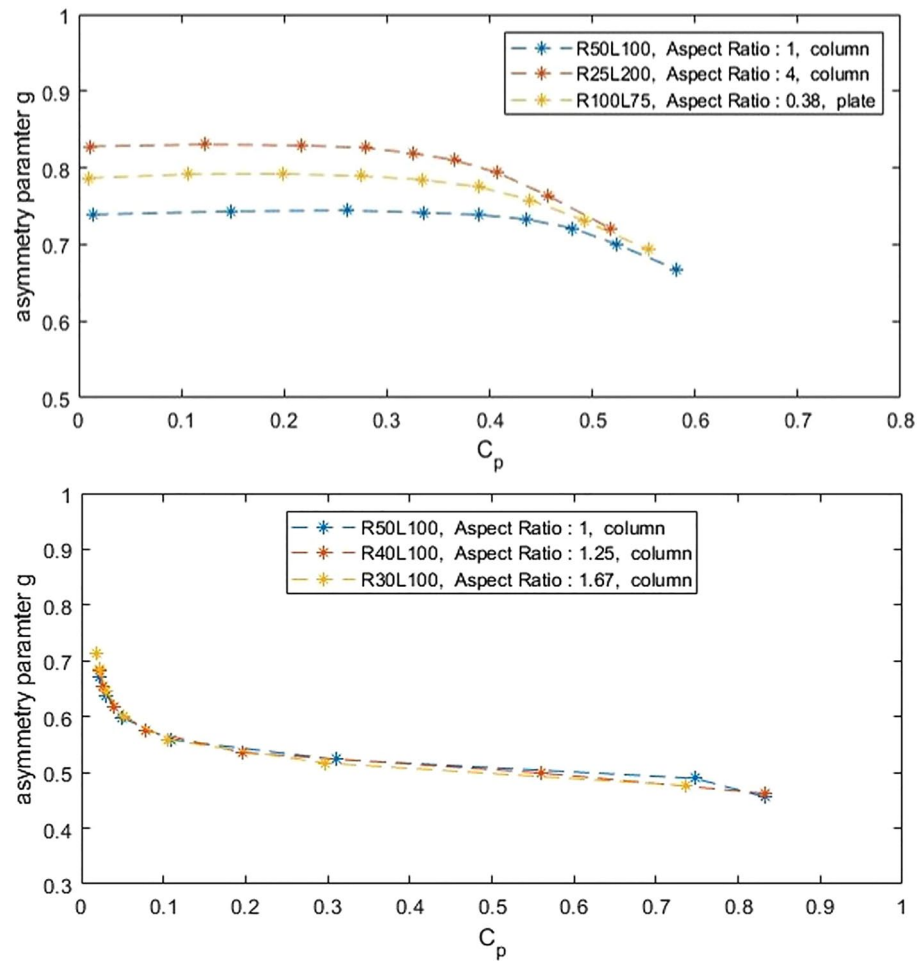


**Figure 6.** (Upper panel) The  $g$ - $C_p$  relation for hexagonal models with distortion parameter variation (Macke, Mueller, & Raschke, 1996). (Lower panel) The  $g$ - $C_p$  relation for smooth ( $\delta = 0$ ) hexagonal models with different mean free path parameter (Macke, Mishchenko, & Cairns, 1996).

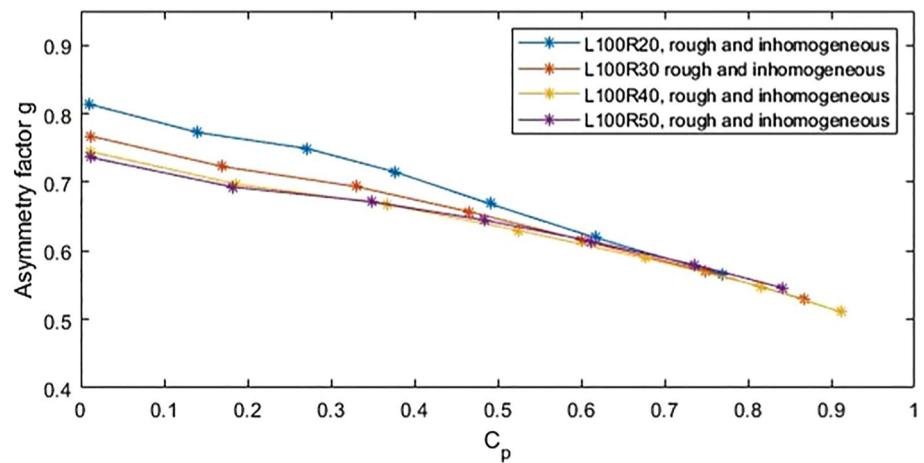


**Figure 7.** The  $g$ - $C_p$  relation for hexagonal models with both increasing distortion parameter and internal scattering (Macke, Mishchenko, & Cairns, 1996; Macke, Mueller, & Raschke, 1996).

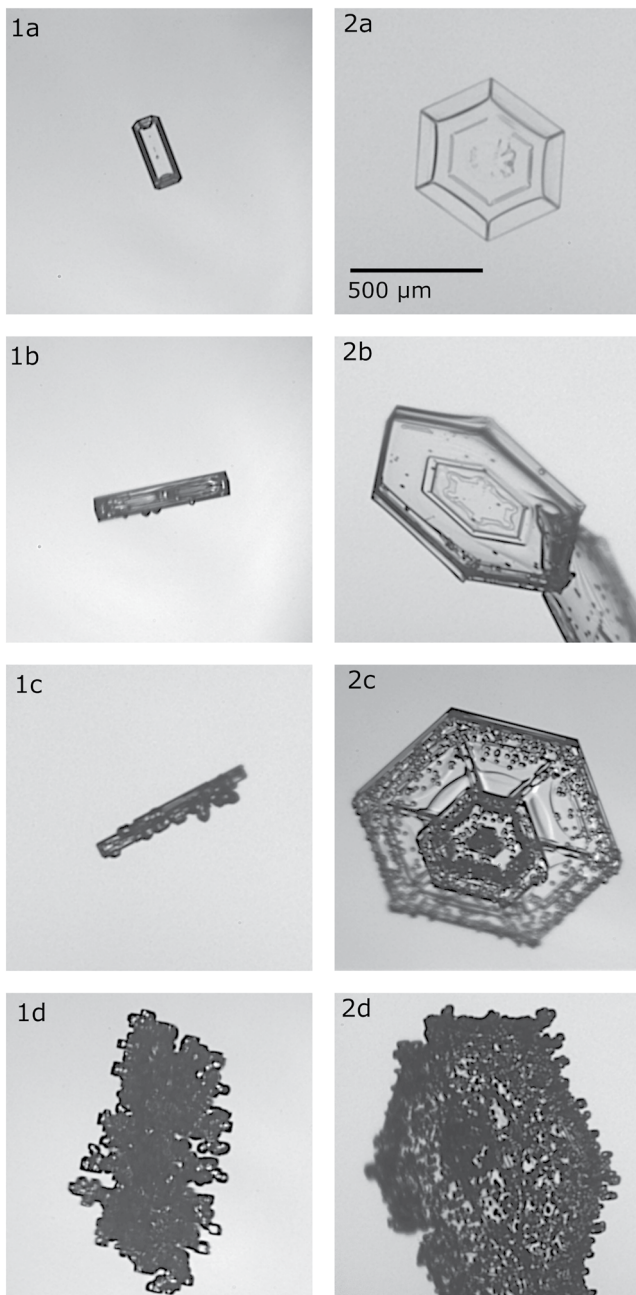


**Figure 8.** Examples of (1) columnar particles and (2) plates with different degrees of riming depending on the surface riming degree (SRD): unrimed (a, SRD = 0%), slightly rimed (b,  $0% < \text{SRD} \leq 25%$ ), moderately rimed (c,  $25 < \text{SRD} \leq 50%$ ) and heavily rimed particles (d,  $50% < \text{SRD} \leq 100%$ ).

the angular light scattering and the morphology of individual cloud particles (Abdelmonem et al., 2016; Schnaiter et al., 2018). Due to this capability, PHIPS is particularly useful when it comes to studying the single-scattering characteristics for particular types of particles.

Here we focus on complex atmospheric particles with visible morphological complexity in the form of riming (i.e., the accretion of supercooled liquid droplets on the surface of ice crystals). Analysis on the category of rimed particles could provide us a convenient way to investigate the relation between particle complexity and their optical scattering properties. This is because the degree of riming is easy to differentiate visually from the PHIPS bright-field stereo-microscopic images due to the high optical resolution of about 3–5  $\mu\text{m}$  (depending on magnification settings) combined with two viewing angles of the same particle. Exemplary ice crystals imaged by PHIPS are shown in Figure 8. It can be seen that the riming can be clearly and reliably be identified and it is possible to estimate the riming degree.

The data presented here comes from observations from high-latitude mixed-phase clouds from the airborne campaigns: the Southern Ocean Clouds, Radiation, Aerosol Transport Experimental Study (SOCRATES) and the Arctic CLoud Observations Using airborne measurements during polar Day (ACLOUD). In these campaigns mostly stratiform mixed-phase clouds were sampled between  $0^\circ\text{C}$  and  $-25^\circ\text{C}$ . Correlated angular light scattering functions and stereo-microscopic images of ice crystals were gathered with the PHIPS probe and the imaged ice crystals were classified according to their riming degree. Three categories for surface riming degree (SRD) were used: slightly rimed (SRD < 25%), moderately rimed (SRD between 25% and 75%) and heavily rimed (SRD > 75%). The classification to the different riming categories was performed by manual inspection. A more detailed discussion on this classification, and on rimed particles in general, can be found in Waitz et al. (2022).

For particles classified in the different riming categories, their  $g$  and  $C_p$  values were derived from the correlated averaged angular light scattering functions. The retrieval algorithm is described in detail in Xu et al. (2022). In summary, a Gaussian quadrature is applied to simultaneously compute the values of  $g$  and  $C_p$ , the accuracy of integration increase as the  $C_p$  value increases. Numerical experiments have been conducted to show the high accuracy of the algorithm, when  $C_p$  is above 0.25 in the case of the PHIPS probe. Besides retrieval uncertainties, another source of uncertainty comes from the nephelometer measurements themselves. Potential uncertainty sources are inuniform coupling of the scattered light to the detector and detector non-uniformity that affects the relative intensities measured by the different detection angles, thus, affecting the asymmetry parameter. The nephelometer was calibrated during a test flight in a haze cloud over the Pacific Ocean where individual spherical droplets were measured (see Figure 12 in Schnaiter et al. (2018)). The measured intensities were compared to a Mie calculation calculated using the droplet sizes retrieved from the stereo-microscopic images. This

was done for a population of droplets to define the relative variation between the scattering channels. Only the first five forward scattering channels were included into the analysis as the side-ward channels showed intensity close to the background due to the light scattering behavior of spherical particles. Using this approach we defined a relative uncertainty of about 3% for the  $g$  and  $C_p$  retrievals.

It was shown recently by Waitz et al. (2022) that up to 50% of ice particles in mixed-phase clouds show riming features. It is expected that simple hexagonal ice crystal models cannot represent the single-scattering properties of rimed crystals. Hence, it will be investigated to which degree conventional models of generating crystal

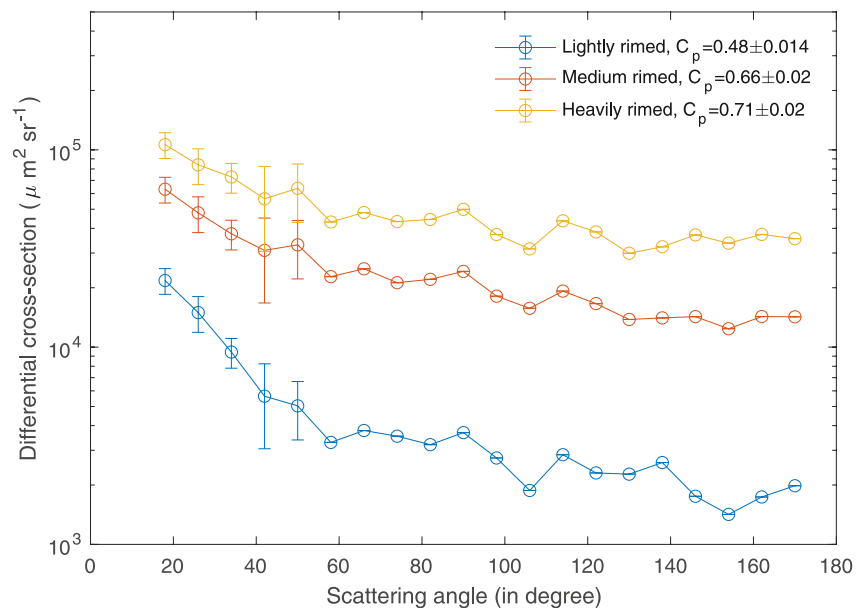


**Figure 9.** The measured mean angular scattering functions of lightly rimed (blue), moderately rimed (red) and heavily rimed (yellow) needles measured by Particle Habit Imaging and Polar Scattering during the Arctic CLOUD Observations Using airborne measurements during polar Day and Southern Ocean Clouds, Radiation, Aerosol Transport Experimental Study campaigns. The error bars for channels 18°, 26°, 34°, 42°, and 50° illustrate the uncertainty of the measurements.

complexity through tilted-facet surface roughness, or by applying air inclusions, can represent the observations by applying the above discussed  $C_p$  -  $g$  space.

Figure 9 shows mean angular scattering functions normalized by particle area deduced from the corresponding stereo images for three groups of needle habits with different riming degrees: slightly rimed (blue), moderately rimed (red) and heavily rimed (yellow) sampled during the ALOUD and SOCRATES campaigns in cloud segments with  $T \geq -17^\circ\text{C}$ . This data set includes 1,126 particles from ALOUD and 226 from SOCRATES. It can be seen that as the riming degree increases, the scattering intensity tends to be more isotropic. In other words, as a particle becomes more rimed, the intensity associated with the forward directions tends to be “directed” to larger scattering angle. Hence the side-scattering increases. This characteristic can be quantitatively measured by computing the  $C_p$  values of the particles, as  $C_p$  values indicate the isotropic degree of the phase functions. As the riming degree increases, the  $C_p$  value increases from 0.48 to 0.71.

To demonstrate the statistical correlation between riming degree and  $C_p$  parameter, we compute the  $C_p$  -  $SRD$  distribution displayed in Figure 10. In doing so, we assume that the  $SRD$  degree is randomly and evenly distributed within each category. One  $C_p$  parameter was calculated for a population of 25 particles and Figure 10 shows the statistical analysis of the  $C_p$  parameter in each of the riming categories. It can be seen that the median  $C_p$  parameter is very well correlated with the  $SRD$  approximately in a linear fashion. As the complexity metric,  $SRD$ , is derived independently from image analysis, such a correlation can be seen as experimental evidence for the effectiveness of using the  $C_p$  parameter in measuring the morphological complexity of ice crystals.

Figure 11 shows the distribution of  $g$ - $C_p$  pairs for all the rimed particles: the blue circles, red circles, and yellow circles represent the  $g$ - $C_p$  pairs for lightly rimed, medium rimed and heavily rimed particles, respectively. In addition, when comparing with simulations using hexagonal model with different ways to induce morphological complexity, we found that the observations can only be explained by a model with both increasing surface roughness and internal scattering (solid lines), even when considering the measurement uncertainty. The dotted curves represent the models using only surface roughness without any inhomogeneity. It can be seen that these models in general give a higher  $g$  that decreases in a non-linear way with respect to  $C_p$ . Although riming on the ice crystals is generally considered as a surface effect, the  $g$ - $C_p$  curves indicate that (a) the surface roughness assumption is inadequate to cause enough flattening of the angular scattering function as indicated by the observations (the measured  $g$  is about 0.03–0.04 lower than surface roughness models for the same  $C_p$ ) or (b) to better model the

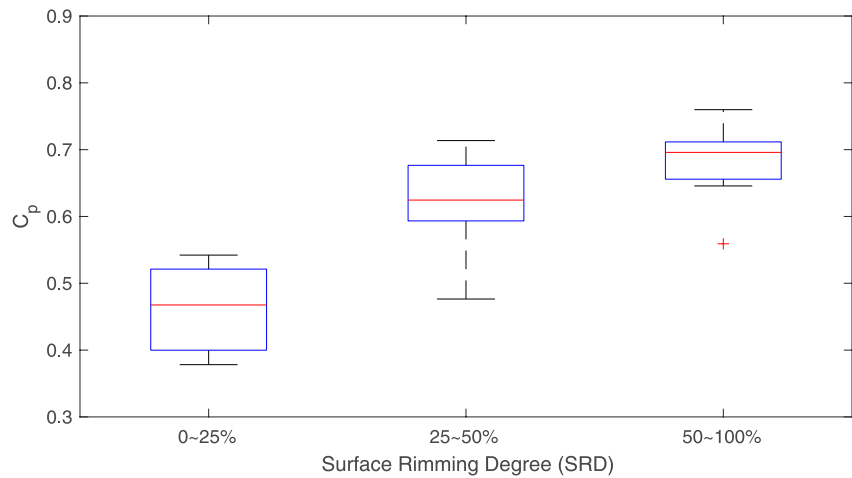


**Figure 10.** The correlation between  $C_p$  and Surface Rimming Degree (SRD). The box plot illustrates the distribution of the  $C_p$  parameter for each category. The red line is the median of the distribution. On each box, the bottom and top edges of the box indicate the 25th and 75th percentiles, respectively. The whiskers extend to the most extreme data points not considered outliers, and the outliers are plotted individually using the “+” marker symbol.

optical scattering properties of rimed crystals, one need to also consider the internal scattering effect due to the inhomogeneity of ice crystals (the measured  $g$ - $C_p$  curves are not consistent with surface roughness models).

## 5. Conclusions

Developing accurate ice crystals light scattering models is important for both climate and remote sensing studies. Nevertheless, this is a challenging task due to not only the technical aspect of computation, but also the complex morphology of natural ice crystals. To better understand the linkages between the morphology and the light scattering properties of real ice crystals, in-situ measurements or laboratory analysis are necessary.

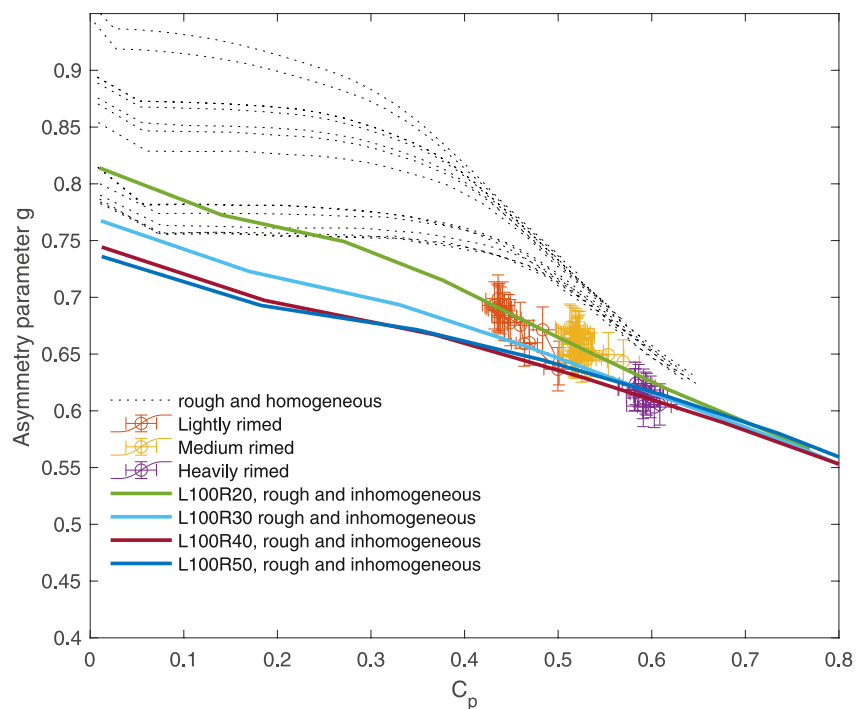


**Figure 11.** The measured  $g$ - $C_p$  relation compared with different models. The error bars show the measurement uncertainty both in  $g$  and  $C_p$ .

In this study, we first discuss some basic properties of the  $C_p$  parameter from theoretical perspectives. Mathematically, the  $C_p$  parameter can be used to measure the local smoothness and overall isotropic degree of a scattering phase function. Under the framework of SOS, it is shown that increased scattering order leads to increased  $C_p$  parameter. We use the  $C_p$  parameter to analyze the scattering phase functions from both surface-roughness and internal-scattering models using geometric-optics ray-tracing methods and found that the  $C_p$  parameter is useful in characterizing and unlocking useful information from the phase functions. With the comparison on  $C_p$  parameter, it is found that particles with aspect ratios of one tend to have higher  $C_p$  than particles with other aspect ratios. Based on simulations, the  $g$ - $C_p$  curves are shown to be useful in differentiating between scattering models, in particular, the surface-roughness models and internal-scattering models.

As an application, we analyze the angular scattering functions of complex atmospheric particles with different SRDs measured in situ. By using a SRD metric, we are able to differentiate ice crystals with varying degrees of complexity from image analysis. The results show that the  $C_p$  parameter is correlated with the riming degree of ice crystals approximately in a linear fashion. In addition, by analyzing the  $g$ - $C_p$  curves of the rimed particles, it is found that the measurement can only be explained by a rough and inhomogeneous model, whereas the surface roughness models with tilted-facets are not consistent with the data.

To summarize, we have demonstrated that the  $C_p$  parameter and its relation to asymmetry parameter  $g$  is helpful for understanding the links between the morphological complexity and the light scattering properties of natural ice crystals. Due to the measurability of the  $C_p$  parameter, it can be used as a useful tool for constraining the light scattering models for ice crystals by in-situ or laboratory measurements.

## Data Availability Statement

The PHIPS single particle scattering data can be found online in the PANGAEA database (<https://doi.org/10.1594/PANGAEA.902611>) for ALOUD (ALOUD, 2022) and the EOL database (<https://doi.org/10.5065/D6639NKQ>) for SOCRATES (SOCRATES, 2022). The single particle microscopic stereo images from those two campaigns are available upon request from the authors. The retrieval algorithm for the asymmetry parameter is written in MATLAB. The code and part of the data is accessible at <https://zenodo.org/badge/latestdoi/440147565>, under a MIT license.

## Acknowledgments

The data were collected using NSF's Lower Atmosphere Observing Facilities, which are managed and operated by NCAR's Earth Observing Laboratory (EOL), and the AWI Polar aircraft. We acknowledge the help of EOL's Research Aviation Facility in campaign preparation and operations. We are grateful to AWI for providing and operating the Polar 6 aircraft during the ALOUD campaign. We thank the crews of both aircrafts, and the technicians of the aircraft for excellent technical and logistical support. This work was funded by the Helmholtz Association's Initiative and Networking Fund (Grant agreement no. VH-NG-1531). Open Access funding enabled and organized by Projekt DEAL.

## References

- Abdelmonem, A., Järvinen, E., Duft, D., Hirst, E., Vogt, S., Leisner, T., & Schnaiter, M. (2016). PHIPS-HALO: The airborne particle habit imaging and polar scattering probe—Part 1: Design and operation. *Atmospheric Measurement Techniques*, 9(7), 3131–3144. <https://doi.org/10.5194/amt-9-3131-2016>
- ALOUD. (2022). Phips single particle scattering data—The Pangea database for acloud [Dataset]. PANGAEA. <https://doi.org/10.1594/pangea.a.902611>
- Baran, A. J. (2012). From the single-scattering properties of ice crystals to climate prediction: A way forward. *Atmospheric Research*, 112, 45–69. <https://doi.org/10.1016/j.atmosres.2012.04.010>
- Baran, A. J., Hill, P., Furtado, K., Field, P., & Manners, J. (2014). A coupled cloud physics–radiation parameterization of the bulk optical properties of cirrus and its impact on the met office unified model global atmosphere 5.0 configuration. *Journal of Climate*, 27(20), 7725–7752. <https://doi.org/10.1175/jcli-d-13-00700.1>
- Baran, A. J., & Labonnote, L.-C. (2007). A self-consistent scattering model for cirrus. I: The solar region. *Quarterly Journal of the Royal Meteorological Society: A Journal of the Atmospheric Sciences, Applied Meteorology and Physical Oceanography*, 133(629), 1899–1912. <https://doi.org/10.1002/qj.164>
- Bi, L., & Yang, P. (2014). Accurate simulation of the optical properties of atmospheric ice crystals with the invariant imbedding T-matrix method. *Journal of Quantitative Spectroscopy and Radiative Transfer*, 138, 17–35. <https://doi.org/10.1016/j.jqsrt.2014.01.013>
- Borovič, A. G., & Grishin, I. A. (2003). Scattering matrices for large ice crystal particles. *JOSA A*, 20(11), 2071–2080. <https://doi.org/10.1364/josaa.20.002071>
- Dodson, B. (1994). *Weibull analysis*. Asq Press.
- Efremenko, D., & Kokhanovsky, A. (2021). *Foundations of atmospheric remote sensing* (pp. 189–192). Springer.
- Groth, S. P., Baran, A. J., Betcke, T., Havemann, S., & Šmigaj, W. (2015). The boundary element method for light scattering by ice crystals and its implementation in bem++. *Journal of Quantitative Spectroscopy and Radiative Transfer*, 167, 40–52. <https://doi.org/10.1016/j.jqsrt.2015.08.001>
- Henyey, L. G., & Greenstein, J. L. (1941). Diffuse radiation in the galaxy. *The Astrophysical Journal*, 93, 70–83. <https://doi.org/10.1086/144246>
- Hess, M., Koelemeijer, R. B., & Stammes, P. (1998). Scattering matrices of imperfect hexagonal ice crystals. *Journal of Quantitative Spectroscopy and Radiative Transfer*, 60(3), 301–308. [https://doi.org/10.1016/S0022-4073\(98\)00007-7](https://doi.org/10.1016/S0022-4073(98)00007-7)
- Hesse, E. (2008). Modelling diffraction during ray tracing using the concept of energy flow lines. *Journal of Quantitative Spectroscopy and Radiative Transfer*, 109(8), 1374–1383. <https://doi.org/10.1016/j.jqsrt.2007.11.002>
- Hioki, S., Yang, P., Baum, B. A., Platnick, S., Meyer, K. G., King, M. D., & Riedi, J. (2016). Degree of ice particle surface roughness inferred from polarimetric observations. *Atmospheric Chemistry and Physics*, 16(12), 7545–7558. <https://doi.org/10.5194/acp-16-7545-2016>

- Järvinen, E., Jourdan, O., Neubauer, D., Yao, B., Liu, C., Andreae, M. O., et al. (2018). Additional global climate cooling by clouds due to ice crystal complexity. *Atmospheric Chemistry and Physics*, 18(21), 15767–15781. <https://doi.org/10.5194/acp-18-15767-2018>
- Järvinen, E., Wernli, H., & Schnaiter, M. (2018). Investigations of mesoscale complexity of small ice crystals in midlatitude cirrus. *Geophysical Research Letters*, 45(20), 11465–11472. <https://doi.org/10.1029/2018GL079079>
- Kleanthous, A., Betcke, T., Hewett, D. P., Escapil-Inchauspé, P., Jerez-Hanckes, C., & Baran, A. J. (2022). Accelerated Calderón preconditioning for Maxwell transmission problems. *Journal of Computational Physics*, 458, 111099. <https://doi.org/10.1016/j.jcp.2022.111099>
- Labonnote, C. L., Brogniez, G., Doutriaux-Boucher, M., Buriez, J.-C., Gayet, J.-F., & Chepfer, H. (2000). Modeling of light scattering in cirrus clouds with inhomogeneous hexagonal monocrystals. Comparison with in-situ and ADEOS-POLDER measurements. *Geophysical Research Letters*, 27(1), 113–116. <https://doi.org/10.1029/1999gl010839>
- Lawson, R., Woods, S., Jensen, E., Erfani, E., Gurganus, C., Gallagher, M., et al. (2019). A review of ice particle shapes in cirrus formed in situ and in anvils. *Journal of Geophysical Research: Atmospheres*, 124(17–18), 10049–10090. <https://doi.org/10.1029/2018jd030122>
- Lenoble, J. (1985). *Radiative transfer in scattering and absorbing atmospheres: Standard computational procedures* (Vol. 300). A. Deepak Hampton.
- Letu, H., Ishimoto, H., Riedi, J., Nakajima, T. Y., Labonnote, L. C., Baran, A. J., et al. (2016). Investigation of ice particle habits to be used for ice cloud remote sensing for the GCOM-C satellite mission. *Atmospheric Chemistry and Physics*, 16(18), 12287–12303. <https://doi.org/10.5194/acp-16-12287-2016>
- Liou, K.-N. (1986). Influence of cirrus clouds on weather and climate processes: A global perspective. *Monthly Weather Review*, 114(6), 1167–1199. [https://doi.org/10.1175/1520-0493\(1986\)114<1167:iocow>2.0.co;2](https://doi.org/10.1175/1520-0493(1986)114<1167:iocow>2.0.co;2)
- Liou, K.-N. (1992). Radiation and cloud processes in the atmosphere. Theory, observation, and modeling (p. 487).
- Liou, K.-N., & Yang, P. (2016). *Light scattering by ice crystals: Fundamentals and applications*. Cambridge University Press.
- Mace, G. G., Zhang, Q., Vaughan, M., Marchand, R., Stephens, G., Trepte, C., & Winker, D. (2009). A description of hydrometeor layer occurrence statistics derived from the first year of merged Cloudsat and CALIPSO data. *Journal of Geophysical Research*, 114(D8), D00A26. <https://doi.org/10.1029/2007jd009755>
- Macke, A., Mishchenko, M. I., & Cairns, B. (1996). The influence of inclusions on light scattering by large ice particles. *Journal of Geophysical Research*, 101(D18), 23311–23316. <https://doi.org/10.1029/96jd02364>
- Macke, A., Mishchenko, M. I., Muinonen, K., & Carlson, B. E. (1995). Scattering of light by large nonspherical particles: Ray-tracing approximation versus T-matrix method. *Optics Letters*, 20(19), 1934–1936. <https://doi.org/10.1364/ol.20.001934>
- Macke, A., Mueller, J., & Raschke, E. (1996). Single scattering properties of atmospheric ice crystals. *Journal of the Atmospheric Sciences*, 53(19), 2813–2825. [https://doi.org/10.1175/1520-0469\(1996\)053<2813:sspoai>2.0.co;2](https://doi.org/10.1175/1520-0469(1996)053<2813:sspoai>2.0.co;2)
- Mano, Y. (2000). Exact solution of electromagnetic scattering by a three-dimensional hexagonal ice column obtained with the boundary-element method. *Applied Optics*, 39(30), 5541–5546. <https://doi.org/10.1364/ao.39.005541>
- Matus, A. V., & L'Ecuyer, T. S. (2017). The role of cloud phase in Earth's radiation budget. *Journal of Geophysical Research*, 122(5), 2559–2578. <https://doi.org/10.1002/2016jd025951>
- McFarquhar, G. M., Yang, P., Macke, A., & Baran, A. J. (2002). A new parameterization of single scattering solar radiative properties for tropical anvils using observed ice crystal size and shape distributions. *Journal of the Atmospheric Sciences*, 59(16), 2458–2478. [https://doi.org/10.1175/1520-0469\(2002\)059\(2458:ANPOSS\)2.0.CO;2](https://doi.org/10.1175/1520-0469(2002)059(2458:ANPOSS)2.0.CO;2)
- Mishchenko, M. I., Travis, L. D., & Lacis, A. A. (2002). *Scattering, absorption, and emission of light by small particles*. Cambridge University Press.
- Mishchenko, M. I., Travis, L. D., & Mackowski, D. W. (1996). T-matrix computations of light scattering by nonspherical particles: A review. *Journal of Quantitative Spectroscopy and Radiative Transfer*, 55(5), 535–575. [https://doi.org/10.1016/0022-4073\(96\)00002-7](https://doi.org/10.1016/0022-4073(96)00002-7)
- Nousiainen, T., & McFarquhar, G. M. (2004). Light scattering by quasi-spherical ice crystals. *Journal of the Atmospheric Sciences*, 61(18), 2229–2248. [https://doi.org/10.1175/1520-0469\(2004\)061\(2229:LSBQIC\)2.0.CO;2](https://doi.org/10.1175/1520-0469(2004)061(2229:LSBQIC)2.0.CO;2)
- Nousiainen, T., & Muinonen, K. (2007). Surface-roughness effects on single-scattering properties of wavelength-scale particles. *Journal of Quantitative Spectroscopy and Radiative Transfer*, 106(1–3), 389–397. <https://doi.org/10.1016/j.jqsrt.2007.01.024>
- Panetta, R. L., Zhang, J.-N., Bi, L., Yang, P., & Tang, G. (2016). Light scattering by hexagonal ice crystals with distributed inclusions. *Journal of Quantitative Spectroscopy and Radiative Transfer*, 178, 336–349. <https://doi.org/10.1016/j.jqsrt.2016.02.023>
- Saito, M., Iwabuchi, H., Yang, P., Tang, G., King, M. D., & Sekiguchi, M. (2017). Ice particle morphology and microphysical properties of cirrus clouds inferred from combined CALIOP-IIR measurements. *Journal of Geophysical Research: Atmospheres*, 122(8), 4440–4462. <https://doi.org/10.1002/2016jd026080>
- Sassen, K., Wang, Z., & Liu, D. (2008). Global distribution of cirrus clouds from CloudSat/Cloud-Aerosol lidar and infrared pathfinder satellite observations (CALIPSO) measurements. *Journal of Geophysical Research*, 113(D8), D00A12. <https://doi.org/10.1029/2008JD009972>
- Schnaiter, M., Järvinen, E., Abdelmonem, A., & Leisner, T. (2018). PHIPS-HALO: The airborne particle habit imaging and polar scattering probe—Part 2: Characterization and first results. *Atmospheric Measurement Techniques*, 11(1), 341–357. <https://doi.org/10.5194/amt-11-341-2018>
- Shcherbakov, V., Gayet, J.-F., Jourdan, O., Minikin, A., Ström, J., & Petzold, A. (2005). Assessment of cirrus cloud optical and microphysical data reliability by applying statistical procedures. *Journal of Atmospheric and Oceanic Technology*, 22(4), 409–420. <https://doi.org/10.1175/JTECH1710.1>
- SOCRATES. (2022). Phips single particle scattering data—The EOL database for socrates [Dataset]. PHIPS. <https://doi.org/10.5065/d6639nqk>
- Stephens, G. L., Tsay, S.-C., Stackhouse, P. W., Jr., & Flatau, P. J. (1990). The relevance of the microphysical and radiative properties of cirrus clouds to climate and climatic feedback. *Journal of the Atmospheric Sciences*, 47(14), 1742–1754. [https://doi.org/10.1175/1520-0469\(1990\)047<1742:trotma>2.0.co;2](https://doi.org/10.1175/1520-0469(1990)047<1742:trotma>2.0.co;2)
- Taflove, A., & Umashankar, K. R. (1990). The finite-difference time-domain method for numerical modeling of electromagnetic wave interactions. *Electromagnetics*, 10(1–2), 105–126. <https://doi.org/10.1080/02726349008908231>
- Tang, G., Panetta, R. L., Yang, P., Kattawar, G. W., & Zhai, P.-W. (2017). Effects of ice crystal surface roughness and air bubble inclusions on cirrus cloud radiative properties from remote sensing perspective. *Journal of Quantitative Spectroscopy and Radiative Transfer*, 195, 119–131. (Laser-Light and Interactions with Particles 2016). <https://doi.org/10.1016/j.jqsrt.2017.01.016>
- Ulanowski, Z., Kaye, P. H., Hirst, E., Greenaway, R. S., Cotton, R. J., Hesse, E., & Collier, C. T. (2014). Incidence of rough and irregular atmospheric ice particles from Small Ice Detector 3 measurements. *Atmospheric Chemistry and Physics*, 14(3), 1649–1662. <https://doi.org/10.5194/acp-14-1649-2014>
- Um, J., & McFarquhar, G. M. (2011). Dependence of the single-scattering properties of small ice crystals on idealized shape models. *Atmospheric Chemistry and Physics*, 11(7), 3159–3171. <https://doi.org/10.5194/acp-11-3159-2011>

- Um, J., McFarquhar, G. M., Hong, Y. P., Lee, S.-S., Jung, C. H., Lawson, R. P., & Mo, Q. (2015). Dimensions and aspect ratios of natural ice crystals. *Atmospheric Chemistry and Physics*, *15*(7), 3933–3956. <https://doi.org/10.5194/acp-15-3933-2015>
- van de Hulst, H. C. (1980). *Multiple light scattering* (p. 739). Elsevier.
- van Diedenhoven, B. (2018). Remote sensing of crystal shapes in ice clouds. In *Springer series in light scattering* (pp. 197–250). Springer. [https://doi.org/10.1007/978-3-319-70808-9\\_5](https://doi.org/10.1007/978-3-319-70808-9_5)
- van Diedenhoven, B. (2021). Variation of ice microphysical properties with temperature and humidity at tops of convective clouds. *Geophysical Research Letters*, *48*(16), e2021GL093673. <https://doi.org/10.1029/2021GL093673>
- Waitz, F., Schnaiter, M., Leisner, T., & Järvinen, E. (2022). In-situ observation of riming in mixed-phase clouds using the PHIPS probe. *Atmospheric Chemistry and Physics*, *22*(11), 7087–7103. <https://doi.org/10.5194/acp-22-7087-2022>
- Wiscombe, W. J. (1980). Improved Mie scattering algorithms. *Applied Optics*, *19*(9), 1505–1509. <https://doi.org/10.1364/ao.19.001505>
- Xu, G., Schnaiter, M., & Järvinen, E. (2022). Accurate retrieval of asymmetry parameter for large and complex ice crystals from in-situ polar nephelometer measurements. *Journal of Geophysical Research: Atmospheres*, *127*(3), e2021JD036071. <https://doi.org/10.1029/2021JD036071>
- Yang, P., Ding, J., Panetta, R. L., Liou, K.-N., Kattawar, G. W., & Mishchenko, M. (2019). On the convergence of numerical computations for both exact and approximate solutions for electromagnetic scattering by nonspherical dielectric particles. *Electromagnetic Waves*, *164*, 27–61. <https://doi.org/10.2528/pier18112810>
- Yang, P., Hioki, S., Saito, M., Kuo, C.-P., Baum, B., & Liou, K.-N. (2018). A review of ice cloud optical property models for passive satellite remote sensing. *Atmosphere*, *9*(12), 499. <https://doi.org/10.3390/atmos9120499>
- Yang, P., & Liou, K. (1996a). Finite-difference time domain method for light scattering by small ice crystals in three-dimensional space. *JOSA A*, *13*(10), 2072–2085. <https://doi.org/10.1364/josaa.13.002072>
- Yang, P., & Liou, K. (1996b). Geometric-optics–integral-equation method for light scattering by nonspherical ice crystals. *Applied Optics*, *35*(33), 6568–6584. <https://doi.org/10.1364/ao.35.006568>
- Yang, P., & Liou, K. (1998). Single-scattering properties of complex ice crystals in terrestrial atmosphere. *Beitrage zur Physik der Atmosphäre-Contributions to Atmospheric Physics*, *71*(2), 223–248.
- Yi, B. (2022). Diverse cloud radiative effects and global surface temperature simulations induced by different ice cloud optical property parameterizations. *Scientific Reports*, *12*(1), 1–11. <https://doi.org/10.1038/s41598-022-14608-w>
- Yi, B., Yang, P., Baum, B. A., L'Ecuyer, T., Oreopoulos, L., Mlawer, E. J., et al. (2013). Influence of ice particle surface roughening on the global cloud radiative effect. *Journal of the Atmospheric Sciences*, *70*(9), 2794–2807. <https://doi.org/10.1175/JAS-D-13-020.1>
- Yurkin, M. A., Hoekstra, A. G., Brock, R. S., & Lu, J. Q. (2007). Systematic comparison of the discrete dipole approximation and the finite difference time domain method for large dielectric scatterers. *Optics Express*, *15*(26), 17902–17911. <https://doi.org/10.1364/oe.15.017902>
- Zhou, C. (2018). Coherent backscatter enhancement in single scattering. *Optics Express*, *26*(10), A508–A519. <https://doi.org/10.1364/oe.26.00a508>